DOI: 10.1021/ma1000173

Macromolecules
ARTICLE

Fracture and Self-Healing in a Well-Defined Self-Assembled Polymer Network

Paulina J. Skrzeszewska,*,†,‡ Joris Sprakel,§ Frits A. de Wolf,⊥ Remco Fokkink,† Martien A. Cohen Stuart,† and Jasper van der Gucht†

†*Laboratory of Physical Chemistry and Colloid Science, Wageningen University and Research Center, Dreijenplein 6, 6703 HB Wageningen, The Netherlands,* ‡*Dutch Polymer Institute (DPI), P.O. Box 902, 5600 AX Eindhoven, The Netherlands,* §*Department of Physics, Harvard University, Cambridge, Massachusetts 02138, and* ⊥*Biobased Products, Agrotechnology & Food Sciences Group, Wageningen University and Research Center, Bornsesteeg 59, 6708 PD Wageningen, The Netherlands*

Received January 5, 2010; Revised Manuscript Received March 1, 2010

ABSTRACT: We studied shear-induced fracture and self-healing of well-defined transient polymer networks formed by telechelic polypeptides, with nodes formed by collagen-like triple helices. When these gels are sheared at a rate that is higher than the inverse relaxation time of the nodes, fracture occurs at a critical stress which increases logarithmically with increasing shear rate. When a constant stress is applied, fracture occurs after a delay time that decreases exponentially with increasing stress. These observations indicate that fracture in these systems is due to stress-activated rupture of triple-helical junctions. After rupture, the physical gels heal completely.

1. Introduction

Physical (transient) gels are solvent-filled networks, formed by reversibly cross-linked polymers, in which weak interactions such as hydrogen bonds, hydrophobic interactions, van der Waals forces, or electrostatic interactions are responsible for cross-links formation. Because of the transient character of the junctions, physical gels, contrary to covalent networks, are able to relax applied stresses by dissociation and re-formation of junctions. This plastic relaxation makes them capable of healing after damage, which is impossible in the case of permanent gels.[1] Consequently, physical networks offer unique advantages for many applications. They can be used as controlled drug delivery systems,[2] rheological regulators in polymer blends,[3] coatings, food, and cosmetics, or as matrix materials for tissue engineering.[4] Also in nature fibrous tissues, such as cartilage, are formed by (partially) noncovalently cross-linked biopolymers. The self-healing capacity of these networks plays an important role in wound healing. Physical gels are viscoelastic, with a characteristic relaxation time that is determined by the lifetime of the physical junctions in the network. When a small stress or strain rate is applied to a physical gel, the natural relaxation mechanism of the material is able to keep up with the deformation, and the system responds linearly. Experiments in this regime, although very useful to understand the internal structure and transient character of the network,[5] often do not correspond to realistic application conditions. Depending on their practical or biological function, hydrogels are exposed to deformations and stresses which go far beyond the linear regime. Under these large deformations, viscoelastic materials can undergo several macroscopic instabilities such as yielding or breaking. While fracture of brittle solids, such as metals or ceramics, has been widely studied, the failure of solvent-filled viscoelastic polymer networks is still poorly understood. So far, most of the work on failure of viscoelastic networks was done for gels formed by classical telechelic polymers, consisting of a hydrophilic chain modified with two hydrophobic end groups,[6−9] or by natural biopolymers.[10−12] However, the internal architecture and the cross-link dynamics are rather poorly defined in most of these systems. This renders understanding the failure process in terms of molecular parameters problematic. To avoid such difficulties, we consider physical gels with very well-defined topology and junction dynamics; these are gels formed by biosynthetic telechelic polypeptides, consisting of rather short collagen-like end blocks $(Pro\text{-}Gly\text{-}Pro)_9$ flanking a water-soluble, random coil-like domain (399 amino acids long).[13] At ambient temperature, the end blocks of this polymer assemble into triple helices,[13] forming a network with a node multiplicity of exactly three.[5] Linear rheology showed that this network obeys, to a good approximation, Maxwell behavior. The relaxation time was found to be in the kiloseconds range and to depend strongly on concentration and temperature, as does the elastic shear modulus.[5] The experimental results could be described quantitatively and without adjustable parameters by an analytical model, based on classical gel theory. This model accounts for the internal gel structure, with bridges, loops, and dangling ends and uses available thermodynamic data for the formation and decay of triple helices.

In this paper, we focus on strongly nonlinear properties such as fracture and self-healing. By carrying out shear start-up experiments, we determine the critical stress for gel failure and the steady-state stress after fracture, both as a function of shear rate. We also investigate delayed network rupture under a fixed applied stress. To get more insight into the mechanism and nature of network disintegration, we carried out particle image velocimetry (PIV). The two-dimensional velocity maps determined from these experiments confirm a shear-induced fracture, which we elaborate in more detail using the activated bond rupture theory proposed by Chaudhury and Evans.[14,15] Finally, we investigate self-healing of the system after rupture by following the recovery of the storage modulus in time. The experiments showed that the system can fully heal after different fracture histories.

*Corresponding author: Tel +31 (0)317-485595; Fax (+31) (0)317 483 777; e-mail paulina.skrzeszewska@wur.nl.

 Published on Web 03/11/2010

2. Materials and Methods

Recombinant Protein. The construction of genes encoding the TR_4T protein with a molecular weight of 42 kDa, the transfection to the production host (the yeast *P. pastoris*), and the production and purification of the protein polymer have been described by Werten et al.[13]

Nonlinear Rheology. All measurements were conducted on an Anton Paar Physica MCR 301 rheometer equipped with a Couette geometry (CC10) with an outer diameter of 10.84 mm and a bob size of 10 mm. Samples were always prepared in the same way. A given amount of protein was dissolved in phosphate buffer (pH 7, I = 10 mM) and then heated at 50 °C for half an hour, allowing the protein to dissolve completely under conditions where no triple helices are formed. Before inserting the warm protein solution in the Couette cell, the geometry was preheated to 50 °C. After lowering the bob, the system was quenched to 20 °C. Prior to actual experiments, the sample was equilibrated for 15 h to form a stable gel. A solvent trap was used to minimize evaporation. Shear start-up experiments were conducted in a wide range of applied shear rates (10^{-6} up to 10^{3} s^{-1}). The stress was monitored for several hours, which is much longer than the relaxation time of the networks (on the order of 1000 s[5]). In an alternative experiment, a constant stress was applied to the sample and the resulting deformation was measured as a function of time.

The network healing was monitored by applying a sinusoidal deformation of small amplitude (frequency ω = 6.28 rad/s and strain γ = 1%) to follow the recovery of the shear modulus (G') in time.

PIV (Particle Image Velocimetry). The local fluid velocity in the gap of the Couette cell is measured by particle image velocimetry (PIV). Tracer particles (0.02% w/v of 10 μm Spherotech Fluorescent Nile Red latex particles) were added to the solution for flow visualization. The set up used to perform PIV is presented in Figure 1. An Anton Paar Physica MCR 300 rheometer was equipped with a Couette cell with transparent walls, with an outer diameter of 36 mm and gap size of 2 mm. A DPSS (diode pump solid state) laser beam with wavelength of 532 nm was passed through two lenses: a spherical lens (Opto Sigma 011-1275; diameter 15 mm, FL 120 mm; Molenaar Optics) and a cylindrical lens (Thorlabs LK1087L2; FL 6.4 mm, H 6.0 mm, L 12.0 mm) in order to generate a laser sheet that illuminates a thin section of the gap in the flow-gradient plane. The estimated thickness of the laser sheet is 155 μm. A CCD camera mounted below the gap records the images, focused on the plane illuminated by the laser sheet. In order to obtain the velocity vectors at each position, two images taken at a given time interval were cross-correlated using a multipass, multigrid FFT algorithm, as implemented in the open source package JPIV.[16] Time intervals were different for different shear rates: 100, 7, 1.4, 0.6, and 0.26 s for $\dot{\gamma}\tau$ = 1.92, 32, 160, 320, and 1600, respectively.

3. Results and Discussion

In this paper, we consider TR_4T solutions at three different concentrations. The values of the plateau storage modulus G'_0 and of the viscoelastic relaxation time τ for these concentrations are given in Table 1. They were determined previously by means of linear creep experiments.[5]

Figure 2 shows the stress response after start-up of steady shear flow for a TR_4T gel at a concentration of 0.96 mM at 20 °C for different applied shear rates. The results are plotted as stress σ versus strain ($\gamma = \dot{\gamma}\tau$). For shear rates below the inverse relaxation time ($\dot{\gamma}\tau < 1$), the stress increases gradually with increasing strain toward its steady-state value. In this regime, the natural relaxation of the transient nodes can keep up with the applied deformation and the material flows homogeneously. However, for higher shear rates, $\dot{\gamma}\tau > 1$, the stress first rises to a pronounced maximum before it decreases rapidly to a lower steady-state value. This decrease in the stress indicates failure of the network. As we will show below, steady-state velocity profiles measured with particle image velocimetry (PIV) show an inhomogeneous flow with a fracture zone. The transient stress curves at high shear rates resemble those for a fracturing brittle solid: an initial elastic response followed by failure at a critical stress. Only for shear rates slightly above the inverse relaxation time ($\dot{\gamma}\tau$ = 3.2 in Figure 2) is some plastic deformation observed, which appears as a quasi-plateau before actual breaking. Note that the stress and strain at which failure occurs depend on the applied shear rate. This is in contrast to observations by Berret[7] for fracture in a network of associative polymers. Recent simulations for a similar system, however, also show such a shear rate dependence.[9] Below we will discuss the kinetics of failure in more detail. First, we consider the initial elastic response.

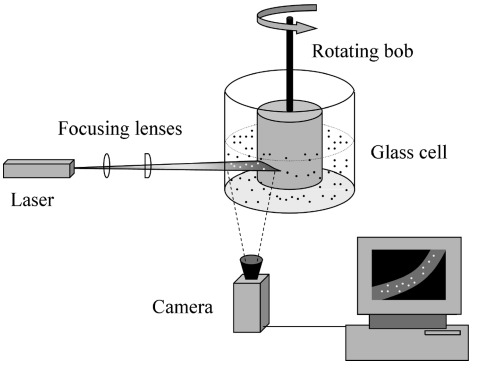

Figure 1. Particle image velocimetry setup.

Table 1. Elastic Plateau Modulus and Relaxation Time for Different TR_4T Concentrations

C_{prot} [mM]	G'_0 [Pa]	τ [s]
0.96	~35	~3200
1.1	~58	~3800
2	~600	~7700

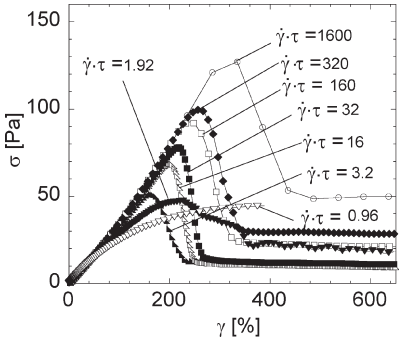

Figure 2. Time-resolved stress response as a function of strain ($\gamma = \dot{\gamma}\tau$) after start-up of steady shear for a 0.96 mM TR_4T gel at 20 °C. The reduced shear rates ($\dot{\gamma}\tau$) are indicated near the lines, with τ equal to 3200 s.

Initial Elastic Response. At low strains, all stress/strain curves in Figure 2 superimpose. Initially, the stress increases linearly with increasing strain with a slope equal to the plateau modulus G'_0. For strains larger than 50%, deviations from the linear response can be observed. At low shear rates ($\dot{\gamma}\tau < 1$), the stress deviates downward because of plastic relaxation in the physical gel (dissociation and re-formation of triple helices). At higher shear rates, there is no such relaxation and the response is purely elastic. In this case, we see that before failure the stress deviates slightly upward,

indicating that the network undergoes weak strain hardening. This strain hardening is probably related to the finite extensibility of the bridging middle blocks. As shown in Figure 3, strain hardening is also observed in oscillatory shear experiments with increasing strain amplitude. For a protein concentration of 0.96 mM, the modulus increases by about 15% with increasing strain before the gel ruptures. At a protein concentration of 2 mM no strain hardening is observed. Probably the regime of strain hardening could not be reached at these higher concentrations because these gels break at much smaller strains. For our system, network stiffening is much weaker than for gels formed by gelatin,[17] silk-collagen-like block polymers,[18] or classical associative telechelics,[6] where the storage modulus increases by as much as a factor 2−5 before fracture occurs. This difference may be due to the fact that we have very long, flexible middle blocks and relatively short node-forming end blocks. This could reduce considerably the nonlinear force−extension relation due to finite chain extensibility.

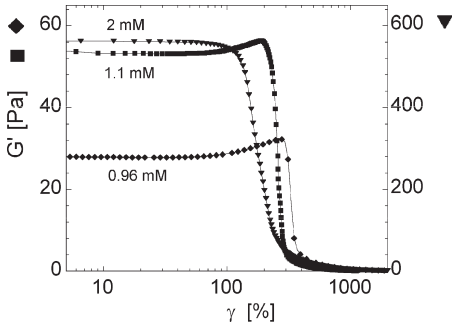

Figure 3. Storage modulus as a function of strain amplitude in an oscillatory shear experiment at a frequency of 6.28 rad/s. Data for 0.96 and 1.1 mM refer to the left axis and those for 2 mM to the right axis.

Fractured Flow at Steady State. After the transient stress response upon start-up of shear flow, the stress finally reaches a steady state (Figure 2). This steady-state stress is plotted as a function of the applied shear rate in Figure 4 for three different TR_4T concentrations at 20 °C (we refer to these plots as "flow curves"). In order to compare gels formed at different protein concentrations, the data from Figure 4A were rescaled by plotting the dimensionless stress σ/G'_0 versus the reduced shear rate $\dot{\gamma}\tau$ (Figure 4B), with G'_0 and τ as given in Table 1.

Along the flow curves several regimes can be observed. At low shear rates, $\dot{\gamma}\tau < 1$, the shear stress increases linearly with the shear rate. The system behaves like a Newtonian liquid with constant zero-shear viscosity. This region was explored in more detail previously.[5] For $\dot{\gamma}\tau$ larger than 1, the flow curves are nonmonotonic: the steady-state stress first decreases with increasing shear rate and then increases again at higher shear rates. This nonmonotonic loop indicates a flow instability with an associated change in structure.[6,19] As discussed above, the transient stress response in this regime is characterized by a large overshoot (Figure 2).

To examine the nature of the failure that occurs at high deformation rates, we measured the velocity profiles in the Couette cell using particle image velocimetry. In Figure 5A, we present snap shots of the velocity field at the steady state for several applied shear rates. At low shear rates, $\dot{\gamma}\tau \sim 1$, the velocity profile is homogeneous: the velocity decreases

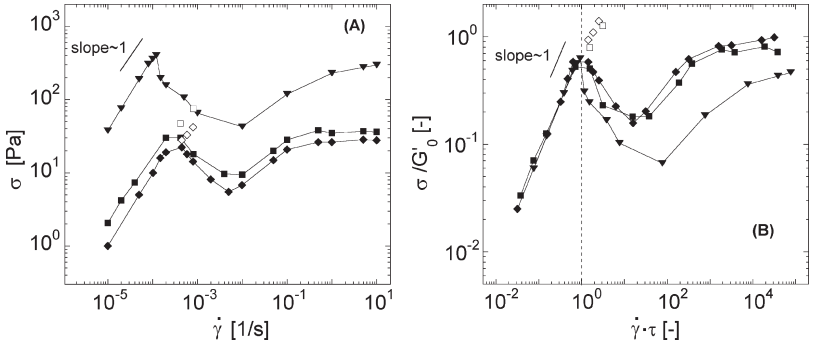

Figure 4. Steady-state flow curves at controlled shear rate for different concentrations (◆) 0.96, (■) 1.1, and (▼) 2 mM. Open symbols denote metastable values. (A) Steady-state shear stress as a function of shear rate. (B) Reduced steady-state shear stress (σ/G'_0) versus reduced shear rate ($\dot{\gamma}\tau$) with G'_0 and τ indicated in Table 1.

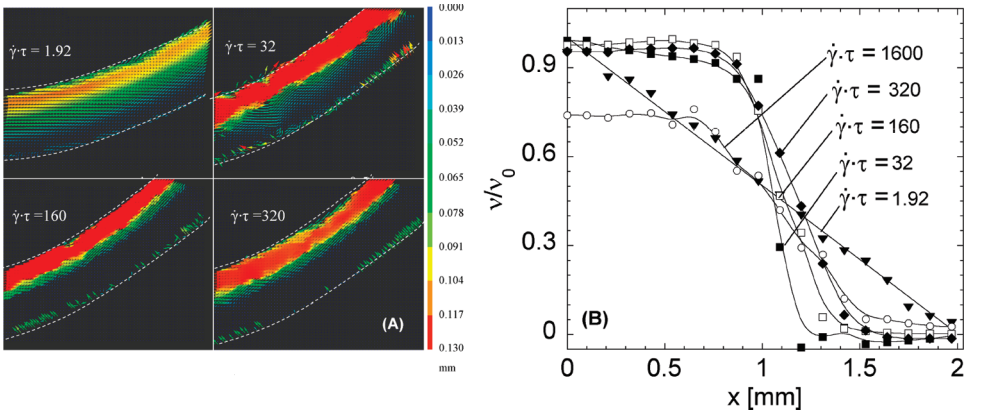

Figure 5. (A) Snapshots of the velocity vector field at the steady state for several applied shear rates (as indicated) for protein concentration 0.96 mM. (A) The color scale indicates the displacement (in mm) of tracked particles between two frames. Time interval between frames: 100 s for $\dot{\gamma}\tau = 1.92$, 7 s for $\dot{\gamma}\tau = 32$, 1.4 s for $\dot{\gamma}\tau = 160$, and 0.6 s for $\dot{\gamma}\tau = 320$. (B) Calculated velocity profiles ($v(x)$) normalized by velocity of the wall (v_0).

linearly from the inner, rotating wall to the outer, stationary wall. At higher shear rates, however, the velocity profile is strongly nonlinear. The gel is broken into two parts: one part close to the moving wall that moves with almost constant velocity and one part at the stationary wall which is not moving at all. In the region between these two phases, the local shear rate is very high. This region is a fracture zone, where all, or most, of the cross-links are ruptured. It can be seen in Figure 5B that this fracture zone has an irregular shape and is rather wide, on the order of a few hundred micrometers, which is much wider than the average distance between cross-links (which is on the order of several nanometers). This was also observed by Berret and Serero in a similar system of telechelic polymers.[6] It indicates that some fluidization occurs in the region where the two gel phases slide past each other. With increasing overall shear rate, the width of the fracture zone increases. The stress in this region, which dominates the macroscopically measured stress, is due to viscous dissipation in the fluidized zone and elastic stresses that arise due to mutual movement of the irregular fracture surfaces. With increasing shear rate, the apparent viscosity decreases, which may indicate that the fracture surfaces become smoother or that the gel locally breaks in smaller fragments.

Note that the position of the fracture zone in the gap is different for every experiment. However, we have never observed it near one of the two walls of the Couette cell (which would result in wall slip). This indicates that the polymer sticks strongly to the Couette wall. Only at very high shear rates (e.g., for $\dot{\gamma}\tau = 1600$ in Figure 5B) we observe some slip at the inner cylinder after the gel has fractured. Before fracture this slip is absent. The position of the fracture zone remains stable for at least 3 h.

Fracture at Constant Applied Stress. Another approach to study the failure of gels is to apply a constant stress and follow the resulting deformation as a function of time. For stresses that are smaller than the elastic modulus G'_0, the gel creeps homogeneously.[5] For larger stresses, however, fracture occurs, leading to an inhomogeneous velocity profile with a very high apparent (overall) shear rate. If the applied stress is much larger than the elastic modulus G'_0, the network fractures almost immediately after applying the load. A different situation is observed for stresses not too far above G'_0. In this case, fracture does not occur immediately but is delayed. Moreover, the delay time is not constant but varies significantly from one experiment to another, suggesting a stochastic fracture mechanism. Some typical creep curves are plotted in Figure 6. Figure 7 shows the time before fracture (t_b) as a function of the applied stress. With increasing stress, the average delay time decreases rapidly.

Delayed fracture has been observed before for soft rubbers, glassy materials, and associative polymer networks.[8,12,20] It has been explained using a crack nucleation model proposed by Pomeau.[21] Essentially, this model is based on Griffith's theory for brittle fracture, which compares the elastic energy released upon crack nucleation to the cohesive energy in the gel.[22] This theory predicts a critical size at which cracks start to grow catastrophically for a given stress. Smaller cracks are stable and do not grow. It was proposed by Pomeau that the crack nucleation time corresponds to the time needed for a crack of this critical size to appear. Associated with this is an energy barrier, which decreases very strongly with the applied stress: $U_a \sim 1/\sigma^4$, so that the rupture time is expected to decrease as $t_b \sim \exp(\text{const}/\sigma^4)$.[8,12,20] Our data in Figure 7 cannot be fitted by such a relation, however (see inset in Figure 7), suggesting that this crack nucleation picture does not apply to our

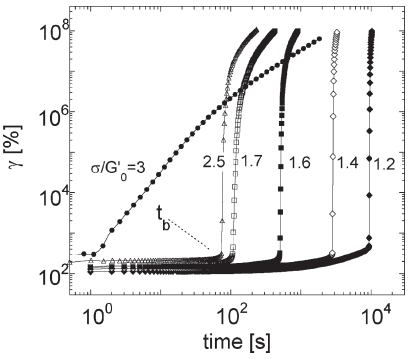

Figure 6. Delayed fracture of a 1.1 mM network at different applied stresses. Initially, the sample responds elastically to the deformation ($\gamma \sim \sigma/G'_0$), but after a lag time t_b, which varies from one experiment to another, the gel breaks, leading to a very rapid increase of the overall strain.

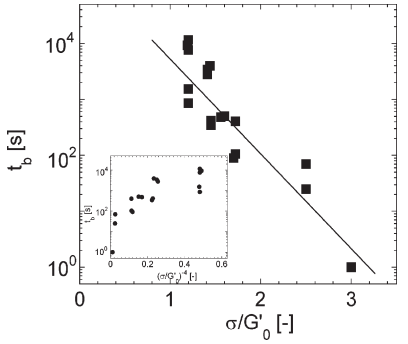

Figure 7. Breaking time (t_b) as a function of the applied stress (σ/G'_0). Inset shows data plotted as t_b versus σ^{-4}.

system. This is furthermore confirmed by our observation that the critical shear stress depends on the applied shear rate (see Figure 2). This cannot be explained by the Griffith theory. It should be kept in mind, however, that the Griffith theory is based on equilibrium considerations, so that it is not clear that it can be applied to dynamic fracture.[23] An alternative approach to describe the dynamics of fracture of polymeric materials is based on activated bond rupture.[14] When a constant stress is applied to the gel, the triple-helical nodes in the gel experience a force f pulling on them. As predicted by Kramers,[15,24] this leads to an enhanced dissociation rate:

$$k_D' = k_D \exp\left[\frac{f\delta}{kT}\right] \quad (1)$$

where k_D is the rate at which elastically active chains relax in the absence of force (equal to $1/\tau$ with τ the linear relaxation time) and δ is a length that characterizes the width of the bond potential. It is on the order of the length of the junction, 9 nm, so that the typical force scale kT/δ is on the order of a few piconewtons.

Because of the presence of defects (small pre-existing cracks) in the network, originating from thermal density fluctuations, the stress is not homogeneous throughout the material. The stress is concentrated near the tip of a pre-existing crack, so that cross-links just ahead of such a crack experience the highest force and therefore the highest dissociation rate. This leads to steady, stress-enhanced propagation of such cracks ("subcritical crack growth"). Once a crack reaches the critical crack size (the so-called Griffith length), catastrophic fracture follows. This model thus

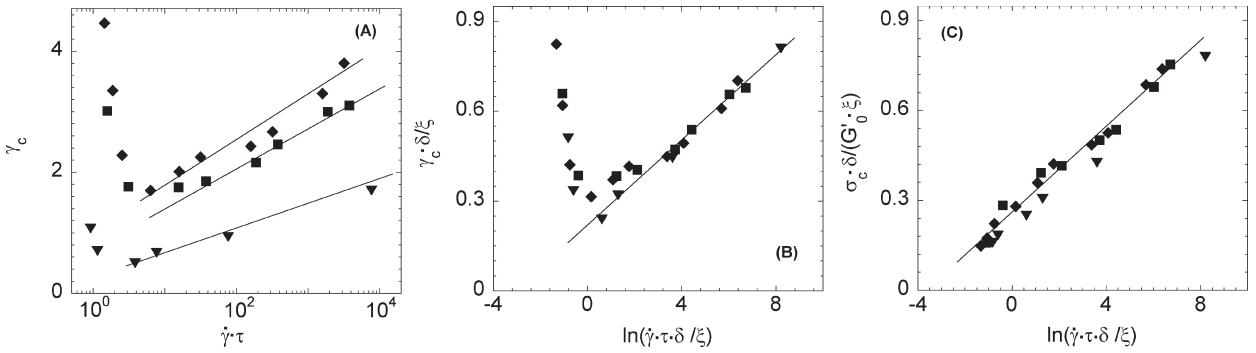

Figure 8. (A) Critical strain as a function of shear rate for different protein concentrations. (B) Renormalized critical strain as as a function of shear rate plotted in the form of eq 5. (C) Same for critical stress. Protein concentrations: (◆) 0.96, (■) 1.1, and (▼) 2 mM.

predicts a rupture time which decreases exponentially with increasing stress:[25,26]

$$t_b \sim 1/k_D' \sim \exp[-\Omega\sigma] \tag{2}$$

where the factor Ω incorporates the factor δ/kT but also takes into account the stress concentration near the pre-existing cracks. As shown in Figure 7, the exponential decrease of t_b with increasing stress agrees well with our data, with $\Omega \approx 3.75/G'_0$. The large scatter in the experimentally determined rupture times reflects the stochastic nature of this process.

Shear Rate Dependence of Rupture. Above, we considered dissociation kinetics under a constant applied force. In order to describe fracture at constant shear rate, we need to account for the fact that the deformation increases linearly with time. Such a description of bond rupture kinetics has been presented by Evans for single bonds[15] and for adhesive rupture by Chaudhury et al.[14] Here, we follow their approach to describe cohesive failure inside the gel. Assuming affine deformation, each bridging chain in the network is stretched by the shear flow at a speed $\xi\dot{\gamma}$, where ξ is the typical distance between junctions in the network. Treating the bridging chains as Gaussian chains with spring constant kT/ξ^2, we find that the force acting on a sheared cross-link increases as $f(t) = K(kT/\xi)\dot{\gamma}t$ (here, we assume that initially, before the shear is started, the force is zero). The factor K accounts for local stress intensification that occurs in the vicinity of the crack tip. Substituting this time-dependent (transient) force into eq 1, we find that the bond dissociation rate increases exponentially with time. The survival probability of a bond $P(t)$ can then be written as[15]

$$P(t) = \exp\{-\int_0^t k_D'[f(t)]\,dt\} = \exp\left\{\frac{\xi}{K\delta\dot{\gamma}\tau}\left[1-\exp\left(\frac{K\delta\dot{\gamma}t}{\xi}\right)\right]\right\} \tag{3}$$

where $\tau = 1/k_D$ is the linear relaxation time.

The average lifetime of a cross-link can be obtained from this as

$$\langle\tau_0'\rangle = \int_0^\infty P(t)\,dt \approx \begin{cases} \tau\left(1-\dfrac{K\delta\dot{\gamma}\tau}{\xi}\right) & \left(\text{if } \dot{\gamma}\tau \ll \dfrac{\xi}{K\delta}\right) \\ \dfrac{\xi}{K\delta\dot{\gamma}}\ln\left(\dfrac{K\delta\dot{\gamma}\tau}{\xi}\right) & \left(\text{if } \dot{\gamma}\tau \gg \dfrac{\xi}{K\delta}\right) \end{cases} \tag{4}$$

In the high shear-rate regime ($\dot{\gamma}\tau \gg 1$), re-formation of cross-links can be neglected. It follows that the gel will undergo a catastrophic rupture after a time $t_b' \approx \langle\tau_0'\rangle$. The critical strain at rupture follows as

$$\gamma_c = \dot{\gamma}t_b' \approx \frac{\xi}{K\delta}\ln\left[\frac{K\delta\dot{\gamma}\tau}{\xi}\right] \tag{5}$$

Hence, the critical strain is predicted to increase logarithmically with increasing shear rate. For $\dot{\gamma}\tau \gg 1$ the stress−strain relation is approximately linear (neglecting the weak strain hardening), so that $\sigma_c/G_0 \approx \gamma_c$ should also increase proportionally to ln $\dot{\gamma}$. Figure 8A shows the critical strain γ_c as a function of $\dot{\gamma}\tau$ for three different concentrations. Indeed, for $\dot{\gamma}\tau > 1$, the critical strain increases logarithmically with increasing shear rate. We now make a more quantitative comparison between experiment and model. As we have shown in our previous paper, the values of G'_0, ξ, and τ depend on the protein concentration (see also Table 1). At low concentrations the network contains many loops and relatively few bridges. Most of these active bridges consist of more than one molecule, so-called superchains.[5] As a result, the modulus G'_0 is low and the typical distance between junctions is large. We estimate the distance ξ between junctions from the modulus using $G'_0 \approx kT/\xi^3$. With increasing concentration it decreases from ~50 nm at 0.96 mM to 20 nm at 2 mM. For the value of δ, we take the length of a triple-helical junction, 9 nm.

To test eq 5, we have plotted $\gamma_c\delta/\xi$ and $(\sigma_c\delta)/(G'_0\xi)$ as a function of $\ln(\gamma\tau\delta/\xi)$ in Figure 8B,C. Indeed, all curves are found to superimpose, and both the critical strain and the critical stress are increasing linearly with the logarithm of the shear rate at sufficiently high deformation rates. Hence, the experimental data are in very good agreement with the model, showing that gel fracture is indeed consistent with a stress-enhanced bond-rupture process. From a fit to eq 5 we find $K \approx 35$, indicating significant stress intensification. At low shear rates ($\dot{\gamma}\tau$ only slightly above unity), deviations from linearity can be observed in Figure 8A,B. The reason for this is that, at these low shear rates, the network can heal by re-formation of triple helices and undergo plastic deformation prior to fracture. This can also be seen in Figure 2 for $\dot{\gamma}\tau = 1.92$, where the stress first remains at a metastable value for some time, before fracture occurs. For $\dot{\gamma}\tau < 1$, no fracture is observed so that the critical strain diverges.

Healing. Contrary to covalently cross-linked gels, physical gels with a finite viscoelastic relaxation time can heal after the deformation is stopped. Figure 9 shows the recovery of the elastic properties after fracturing it by applying a constant shear rate (A) or shear stress (B). The system can recover up to 100% of its initial elastic properties, even after

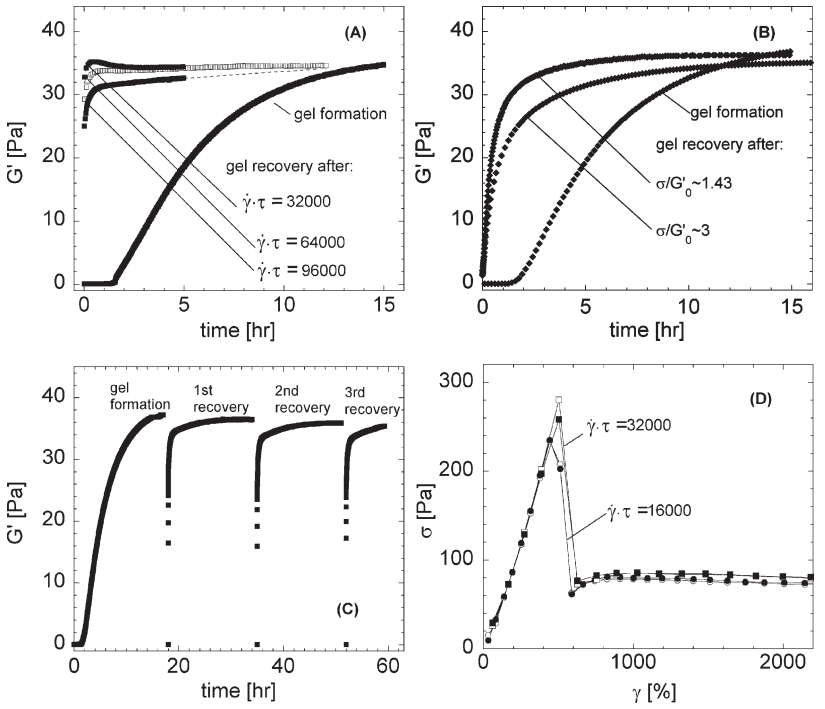

Figure 9. Healing of 0.96 mM gel after different fracture histories: (A) Storage modulus recovery after 1 h of shearing with different shear rates (as indicated). (B) Recovery after applying stress of 50 and 105 Pa for half an hour. (C) Multiple fracture-recovery cycles (with $\dot{\gamma}\tau$ = 96 000). (D) Recovery of the fracture strength after fracture and healing for two shear rates. Filled symbols: before fracture; open symbols: after fracture followed by self-healing.

several fracturing cycles (Figure 9C). Not only the storage modulus is recovered but also the fracture strength: after healing the gel can be strained to the same maximum strain and stress (Figure 9D). We compare the kinetics of healing after rupture to the kinetics of gel formation upon cooling, which we investigated in detail previously.[27] The latter is characterized by a lag phase before elastic properties start to appear (see Figure 9A−C). This lag phase is consistent with the fact that at least 50−60% of the end blocks should be involved in elastically active junctions[27] before a percolated network appears. Until that point, the storage modulus is almost undetectable.

In the curves that show the recovery after fracture, no such lag phase is observed and the storage modulus comes back to its original plateau value within ~1 h after shearing or ~5 h after applying stress. This is much faster than the initial gel formation upon cooling. This indicates that outside the fracture zone the junctions have not appreciably dissociated during the fracture processes. Healing then only requires the reformation of junctions that connect the undamaged pieces of network (gel clusters). Also, the formation of loops may be less likely in the fracture zone because the second end of the same molecule is probably already connected to a floating piece of gel. Consequently, re-formation of the same amount of triple helices leads to a more effective increase of the elastic properties.

The rate of recovery $(dG'/dt)_0$ during healing depends on the applied deformation history. When the gel is fractured at a higher applied shear rate or stress, the recovery is slower (Figure 9A,B). As shown in Figure 5B, higher shear rates result in a wider fracture zone, which requires more time to heal.

4. Concluding Remarks

In this paper we have investigated the failure of physical networks formed by collagen-inspired telechelic polypeptides with well-defined node multiplicity. When a constant shear rate or shear stress is applied to these physical gels, the system undergoes a macroscopic fracture. This instability could be observed with PIV. The kinetics of fracture strongly suggest that gel fracture is due to stress-activated rupture of triple-helical nodes in the network. When the applied stress or shear rate is taken away, the network recovers completely. The kinetics of this self-healing is much faster than the initial sol−gel transition upon cooling of a protein solution.

A similar shear-induced fracture has been observed in other transient polymer networks, formed by telechelic polymers with hydrophobic associating groups.[7,8] In these systems, the critical strain at which the gel ruptures was found not to depend on the applied shear rate,[7] although the range of applied shear rates was not as large as in the present study. The critical rupture stress in these systems could be estimated using a quasi-static fracture model, based on classical Griffith theory. By contrast, our measurements do show a shear rate dependence of the critical rupture strain. This cannot be explained with the static Griffith model and strongly suggests a dynamic fracture process that is governed by stress-activated bond rupture. We have no explanation for the different behaviors found in these transient networks. Possibly, the much longer relaxation time of our triple helix-based networks leads to more solidlike behavior. We note that a similar shear rate dependence was found in coarse-grained Brownian dynamics simulations on failure in transient polymer networks.[9]

Acknowledgment. We thank Robert Molenaar for his advice concerning the optics for the PIV setup. This research forms part of the research program of the Dutch Polymer Institute (DPI) project #602. J.S. thanks The Netherlands Organization for Scientific Research (NWO) for financial support.

References and Notes

(1) Wang, Q.; Mynar, J. L.; Yoshida, M.; Lee, E.; Lee, M.; Okuro, K.; Kinbara, K.; Aida, T. *Nature* **2010**, *463* (7279), 339−343.
(2) Sutter, M.; Siepmann, J.; Hennink, W. E.; Jiskoot, W. *J. Controlled Release* **2007**, *119* (3), 301–312.

(3) Kim, J.; Kim, S. S.; Kim, K. H.; Jin, Y. H.; Hong, S. M.; Hwang, S. S.; Cho, B. G.; Shin, D. Y.; Im, S. S. *Polymer* **2004**, *45* (10), 3527–3533.
(4) Kim, B. S.; Mooney, D. J. *J. Biomed. Mater. Res.* **1998**, *41* (2), 322–332.
(5) Skrzeszewska, P. J.; de Wolf, F. A.; Werten, M. W. T.; Moers, A. P. H. A.; Stuart, M. A. C.; van der Gucht, J. *Soft Matter* **2009**, *5* (10), 2057–2062.
(6) Berret, J. F.; Sereo, Y.; Winkelman, B.; Calvet, D.; Collet, A.; Viguier, M. *J. Rheol.* **2001**, *45* (2), 477–492.
(7) Berret, J. F.; Serero, Y. *Phys. Rev. Lett.* **2001**, *87* (4), 048303−1–4.
(8) Tabuteau, H.; Mora, S.; Porte, G.; Abkarian, M.; Ligoure, C. *Phys. Rev. Lett.* **2009**, *102* (15).
(9) Sprakel, J.; Spruijt, E.; van der Gucht, J.; Padding, J. T.; Briels, W. J. *Soft Matter* **2009**, *5* (23), 4748–4756.
(10) Baumberger, T.; Caroli, C.; Martina, D. *Eur. Phys. J. E* **2006**, *21* (1), 81–89.
(11) Baumberger, T.; Ronsin, O. *J. Chem. Phys.* **2009**, *130* (6).
(12) Bonn, D.; Kellay, H.; Prochnow, M.; Ben-Djemiaa, K.; Meunier, J. *Science* **1998**, *280* (5361), 265–267.
(13) Werten, M. W. T.; Teles, H.; Moers, A.; Wolbert, E. J. H.; Sprakel, J.; Eggink, G.; de Wolf, F. A. *Biomacromolecules* **2009**, *10* (5), 1106–1113.
(14) Chaudhury, M. K. *J. Phys. Chem. B* **1999**, *103* (31), 6562–6566.
(15) Evans, E.; Ritchie, K. *Biophys. J.* **1997**, *72* (4), 1541–1555.
(16) http://www.jpiv.vennemann-online.de/download.html.
(17) Bot, A.; van Amerongen, I. A.; Groot, R. D.; Hoekstra, N. L.; Agterof, W. G. M. *Polym. Gels Networks* **1996**, *4* (3), 189–227.
(18) Martens, A. A.; van der Gucht, J.; Eggink, G.; de Wolf, F. A.; Stuart, M. A. C. *Soft Matter* **2009**, *5* (21), 4191–4197.
(19) Sprakel, J.; Spruijt, E.; Stuart, M. A. C.; Besseling, N. A. M.; Lettinga, M. P.; van der Gucht, J. *Soft Matter* **2008**, *4* (8), 1696–1705.
(20) Shahidzadeh-Bonn, N.; Vie, P.; Chateau, X.; Roux, J. N.; Bonn, D. *Phys. Rev. Lett.* **2005**, *95* (17).
(21) Pomeau, Y. *C. R. Acad. Sci., Ser. II* **1992**, *314* (6), 553–556.
(22) Griffith, A. A. *Philos. Trans. R. Soc. London, Ser. A* **1921**, *221* (221), 163–198.
(23) Gan, Y. *Phys. Rev. Lett.* **2006**, *96* (25).
(24) Kramers, H. A. *Physica* **1940**, *7* (7), 284–304.
(25) Zhurkov, S. N. *Int. J. Fract.* **1984**, *26* (4), 295–307.
(26) Santucci, S.; Vanel, L.; Ciliberto, S. *Eur. Phys. J.—Spec. Top.* **2007**, *146*, 341–356.
(27) Skrzeszewska, P. J.; de Wolf, F. A.; Stuart, M. A. C.; van der Gucht, J. *Soft Matter* **2010**, *6* (2), 416–422.